Research Square

Preprints are preliminary reports that have not undergone peer review.
They should not be considered conclusive, used to inform clinical practice,
or referenced by the media as validated information.

GRP75-Mediated Mitochondria-Endoplasmic Reticulum Contacts Modulate Mitochondrial Ca2+ Signalling and Apoptotic Sensitivity to Sorafenib in HepG2 Cells

Xiaoling Zhou
The First Affiliated Hospital of Guangxi University of Chinese Medicine
Zhuchun Jiang
The People's Hospital of Hezhou
Liyan Chen
The People's Hospital of Hezhou
Jialing Liu
Guangxi University of Chinese Medicine
Qionghui Huang
Guangxi University of Chinese Medicine
Lin Liu
Guangxi University of Chinese Medicine
Baihan Liu
Guangxi University of Chinese Medicine
Yuhua Yan
Guangxi University of Chinese Medicine
Ding Zhang
1301482056@qq.com

The First Affiliated Hospital of Guangxi University of Chinese Medicine

Research Article

Keywords: hepatocellular carcinoma, GRP75/HSPA9, mitochondria-endoplasmic reticulum contacts, MERCs, mitochondrial Ca2 + signalling, mitochondrial apoptosis, sorafenib sensitivity

Posted Date: November 9th, 2026

DOI: https://doi.org/10.21203/rs.3.rs-10649973/v1

License: This work is licensed under a Creative Commons Attribution 4.0 International License.
Read Full License

Additional Declarations: No competing interests reported.

Abstract

Background

Systemic treatment for hepatocellular carcinoma (HCC) remains limited by incomplete therapeutic responses and dysregulated apoptosis. Mitochondria-endoplasmic reticulum contacts (MERCs) coordinate Ca2 + signalling, mitochondrial function and cell-death control. GRP75, encoded by HSPA9 and also known as mortalin, is a molecular chaperone in the IP3R-GRP75-VDAC1 complex. However, whether GRP75-mediated MERC remodelling directly links mitochondrial Ca2 + responses to sorafenib sensitivity in HCC cells remains unclear.

Methods

Transmission electron microscopy (TEM) was used to compare MERC morphology between HepG2 cells and non-malignant THLE-2 liver epithelial cells. HSPA9 mRNA expression and its association with survival were analysed in the TCGA-LIHC cohort. GRP75-overexpressing and GRP75-knockdown HepG2 cells were assessed for MERC morphology, mitochondrial Ca2 + transients measured with Rhod-2 AM, JC-1-labelled mitochondrial membrane potential, Annexin V-FITC/PI apoptosis, apoptotic marker expression and Caspase-3/7 activity. A HepG2 xenograft model, together with HSPA9/GRP75 qPCR and immunohistochemistry, was used to examine the relationship between GRP75 knockdown, endpoint tumour burden, and sorafenib-associated apoptotic markers in vivo.

Results

Compared with THLE-2 cells, HepG2 cells showed a greater fraction of the mitochondrial perimeter occupied by MERCs and a shorter mean contact distance. In TCGA-LIHC, HSPA9 mRNA was upregulated in HCC tumour tissues and was associated with worse overall survival. GRP75 overexpression increased MERC contact length and reduced mean contact distance, whereas GRP75 knockdown had the opposite effect. Rhod-2 AM assays showed enhanced mitochondrial Ca2 + transients in GRP75-overexpressing cells and weaker transients in GRP75-knockdown cells. Upon sorafenib challenge, GRP75 knockdown increased apoptosis, aggravated mitochondrial membrane-potential loss, increased Bax and cleaved caspase-3 expression, reduced Bcl-2 expression and elevated Caspase-3/7 activity. Conversely, GRP75 overexpression conferred a relative protective effect against sorafenib-induced mitochondrial injury. In the HepG2 xenograft model, GRP75 knockdown was associated with lower final tumour burden and reduced Ki-67 immunoreactivity. Combined treatment with sorafenib further increased cleaved caspase-3 immunoreactivity.

Conclusions

GRP75 expression was associated with MERC remodelling in HepG2 cells and parallel alterations in mitochondrial Ca2 + transients, mitochondrial membrane-potential maintenance and apoptotic sensitivity to sorafenib. Together, the in vitro and in vivo data suggest that the GRP75-MERC axis primes the mitochondrial apoptotic threshold following drug exposure. Additional cell models, GRP75 rescue experiments and dynamic Ca2+-flux analyses are needed to establish the causal mechanism.

Background

Hepatocellular carcinoma (HCC) is a major cause of cancer-related death worldwide, and its disease burden, epidemiological patterns and prevention needs continue to change [1–3]. The diagnostic and therapeutic framework for HCC, especially systemic therapy, has expanded substantially in recent years [4–6]. Sorafenib established targeted therapy as a treatment option for advanced HCC [7, 8]. Later, immunotherapy-based combinations, including atezolizumab plus bevacizumab, reshaped first-line treatment and renewed interest in mechanisms of response and resistance [9–13]. Despite these advances, inadequate response, acquired progression and limited long-term benefit remain major clinical challenges [14, 15]. Although sorafenib is no longer the only first-line option in all settings, it remains a useful model for studying mitochondrial injury, stress adaptation and apoptotic-threshold regulation in HCC under therapeutic stress.

Tumour-cell adaptation to therapeutic stress depends not only on canonical oncogenic signalling but also on structural and functional communication between organelles. Mitochondria-endoplasmic reticulum contacts (MERCs), also known as mitochondria-associated endoplasmic reticulum membranes (MAMs), are subcellular platforms for local signal integration between the endoplasmic reticulum (ER) and mitochondria [16–19]. At these sites, Ca2 + released from the ER can be taken up by adjacent mitochondria, influencing mitochondrial metabolism, membrane-potential stability and the threshold for apoptosis initiation [16, 20]. Recent studies have also implicated ER-mitochondria contacts in lipid peroxidation, ferroptosis and MAM-dependent cell-death regulation [21, 22]. The structural state of MERCs may therefore influence tumour-cell fate after drug treatment.

GRP75 (glucose-regulated protein 75), encoded by HSPA9 and also known as mortalin, is a molecular chaperone that links ER and mitochondrial Ca2 + signalling. A classic study showed that GRP75 bridges the ER Ca2+-release channel IP3R with the mitochondrial outer-membrane channel VDAC1, forming the IP3R-GRP75-VDAC1 complex and supporting ER-mitochondria Ca2 + coupling [23]. However, this complex represents only one component of the Ca2+-regulatory network at ER-mitochondria contact sites [24]. In metabolic-stress models, GRP75 contributes to ER-mitochondria coupling, mitochondrial functional regulation and apoptosis-related processes [25]. In tumour models, GRP75-associated MAM integrity has also been proposed to affect chemotherapy-induced mitochondrial dysfunction and apoptotic responses [26].

In HCC, evidence increasingly supports a disease-related role for HSPA9/mortalin/GRP75. 27-Hydroxycholesterol can promote multidrug resistance in HCC by regulating GRP75-associated redox

balance and metabolic reprogramming [27]. Mortalin-regulated changes in protein phosphorylation have also been used to explain its potential contribution to HCC progression [28]. Interactions between mortalin and proteins such as p53 are considered possible therapeutic targets in cancer [29]. Recent studies have further associated GRP75 with HCC drug resistance, targeted intervention and VDAC1-related ER-mitochondria interactions [30, 31]. In sorafenib-treated HCC cells, cell-death and resistance states can also be influenced by ER stress, RAF1/MEK/ERK signalling, BCL-2 family proteins and ER-mitochondria crosstalk [32–35]. However, whether GRP75-mediated MERC remodelling directly links mitochondrial Ca2 + responses to sorafenib sensitivity remains unclear.

Here, we investigated whether GRP75-associated MERC remodelling links mitochondrial Ca2 + responses to apoptotic sensitivity to sorafenib. First, we compared MERC morphology between HepG2 cells and non-malignant THLE-2 liver epithelial cells and analysed HSPA9 mRNA expression and survival associations in the TCGA-LIHC cohort. We then manipulated GRP75 expression by overexpression or knockdown and assessed MERC morphology, mitochondrial Ca2 + transients, mitochondrial membrane potential, apoptosis, apoptotic marker expression and Caspase-3/7 activity. Finally, we used a HepG2 xenograft model to examine the relationship between GRP75 knockdown, endpoint tumour burden, and sorafenib-associated apoptotic markers.

Methods

Cell culture and main reagents

The human HCC cell line HepG2 and the human non-malignant liver epithelial cell line THLE-2 were purchased from Procell Life Science & Technology Co., Ltd. (Wuhan, China). HepG2 cells were cultured in high-glucose Dulbecco's modified Eagle medium (DMEM; Gibco, Grand Island, NY, USA) supplemented with 10% fetal bovine serum (FBS; Gibco), 100 U/mL penicillin and 100 microg/mL streptomycin (Gibco). THLE-2 cells were cultured in THLE-2-specific medium (Procell) supplemented with growth-factor additives and 10% FBS according to the manufacturer's instructions. Before seeding THLE-2 cells, culture flasks were coated at 37°C for 2 h or overnight with coating solution containing 0.01 mg/mL fibronectin, 0.03 mg/mL type I collagen and 0.01 mg/mL bovine serum albumin (BSA). All cells were maintained at 37°C in a humidified incubator with 5% CO2 and were passaged with 0.25% trypsin-EDTA (Procell) when they reached 80-90% confluence.

Rabbit monoclonal antibodies against GRP75 (HSPA9; ab2799), Bax (ab32503), Bcl-2 (ab182858) and cleaved caspase-3 (ab32042), as well as a mouse monoclonal antibody against beta-actin (ab205), were purchased from Abcam (Cambridge, UK). Goat anti-rabbit and goat anti-mouse horseradish peroxidase (HRP)-conjugated secondary antibodies were also purchased from Abcam. DAPI dye and Lipofectamine 3000 transfection reagent were purchased from Invitrogen (Carlsbad, CA, USA). Sorafenib was purchased from Selleck Chemicals (Houston, TX, USA).

Plasmid construction and cell transfection

To construct the GRP75 overexpression vector, the full-length coding sequence of human GRP75 was cloned into the pcDNA3.1(+) vector (Invitrogen), generating the recombinant pcDNA3.1-GRP75 plasmid. For GRP75 knockdown, two short hairpin RNA (shRNA) sequences targeting different regions of HSPA9/GRP75 (shGRP75-1 and shGRP75-2) were designed and ligated into the pLKO.1-puro vector (Addgene, Cambridge, MA, USA). A shRNA sequence not targeting any known human gene was used as the negative control (shNC). All plasmids were verified by Sanger sequencing.

Before transfection, HepG2 cells were seeded in 6-well plates. When cells reached 60-70% confluence, pcDNA3.1-GRP75 or shGRP75 plasmids were transfected according to the Lipofectamine 3000 instructions. Cells were collected 48 h after transfection for subsequent experiments, or stable knockdown cell lines were selected using 2 microg/mL puromycin. The shGRP75 sequence with the higher knockdown efficiency was used for subsequent functional assays.

RNA extraction and quantitative real-time PCR

Total RNA was extracted from treated cells or tumour tissues using TRIzol reagent (Invitrogen). RNA concentration and purity were determined using a NanoDrop 2000 spectrophotometer (Thermo Fisher Scientific, Waltham, MA, USA). Subsequently, 1 microg of total RNA was reverse-transcribed into cDNA using PrimeScript RT Master Mix (TaKaRa, Wuhan, China).

Quantitative real-time PCR (qRT-PCR) was performed on an ABI 7500 Real-Time PCR System (Applied Biosystems, Foster City, CA, USA) using SYBR Premix Ex Taq II (TaKaRa). The PCR programme consisted of initial denaturation at 95°C for 30 s, followed by 40 cycles of denaturation at 95°C for 5 s and annealing/extension at 60°C for 34 s. Beta-actin (ACTB) was used as the internal reference gene, and relative HSPA9/GRP75 mRNA expression was calculated using the $2^{-\Delta\Delta Ct}$ method. Primer sequences are provided in Supplementary Table 2.

Western blot analysis

Total cellular protein was extracted using RIPA lysis buffer containing protease and phosphatase inhibitors (Solarbio, China), and protein concentrations were measured using a BCA protein assay kit (Solarbio). Protein samples (30 microg per lane) were separated by 10% or 12% SDS-PAGE and transferred onto polyvinylidene fluoride (PVDF) membranes (Millipore, Billerica, MA, USA). PVDF membranes were blocked with TBST containing 5% non-fat milk for 1 h at room temperature and then incubated with primary antibodies overnight at 4°C. Primary antibody dilutions were as follows: GRP75 (1:1000), Bax (1:1000), Bcl-2 (1:1000), cleaved caspase-3 (1:1000) and beta-actin (1:2000). The next day, membranes were washed with TBST and incubated with HRP-conjugated secondary antibodies (1:5000) for 1 h at room temperature. Protein bands were developed using enhanced chemiluminescence (ECL) reagent (Millipore), and images were acquired using a ChemiDoc XRS+ imaging system (Bio-Rad, Hercules, CA, USA).

Transmission electron microscopy

After cell pellets were collected, samples were fixed in 2.5% glutaraldehyde at 4°C for 2 h and washed with phosphate-buffered saline (PBS). Samples were then post-fixed with 1% osmium tetroxide for 1 h. After dehydration through graded ethanol solutions of 50%, 70%, 90% and 100%, samples were embedded in epoxy resin. Ultrathin sections of 70 nm were prepared using a Leica EM UC7 ultramicrotome (Leica, Wetzlar, Germany) and double-stained with uranyl acetate and lead citrate. Images were observed and captured using a Hitachi H-7650 transmission electron microscope (Hitachi, Tokyo, Japan) at an accelerating voltage of 80 kV.

At least 20 cells were randomly selected for analysis from each sample. Contact length and contact distance between mitochondria and the ER were measured, and MERC contact length was calculated as a percentage of the mitochondrial perimeter to quantify the degree of structural coupling between mitochondria and the ER.

Rhod-2 AM assay for mitochondrial Ca2+ transients

HepG2 cells were seeded in confocal culture dishes. For detection, cells were incubated with 5 microM Rhod-2 AM (Thermo Fisher Scientific) in serum-free medium at 37°C for 30 min. After washing, cells were placed in a Leica SP8 confocal live-cell imaging system. Basal fluorescence intensity was recorded first, followed by addition of 100 microM ATP to stimulate IP3 production and induce ER Ca2+ release. Changes in Rhod-2 AM fluorescence intensity were continuously recorded for 5 min after ATP stimulation.

For analysis, mitochondrial regions in each cell were defined as regions of interest (ROIs). The difference between peak fluorescence intensity after stimulation and basal fluorescence intensity (Delta F) was divided by basal fluorescence intensity (F0) to obtain Delta F/F0. This value, representing the Rhod-2 AM fluorescence transient, was used to quantify mitochondrial Ca2+ uptake.

Annexin V-FITC/PI apoptosis analysis

Cell apoptosis was detected by flow cytometry using an Annexin V-FITC/propidium iodide (PI) apoptosis detection kit (BD Biosciences, San Jose, CA, USA). HepG2 cells from different treatment groups were collected after exposure to 10 microM sorafenib for 24 h and washed twice with pre-cooled PBS. Cells were resuspended in Binding Buffer and incubated with Annexin V-FITC and PI for 15 min at room temperature in the dark according to the kit instructions. Cells were then analysed by flow cytometry, and data were processed using CellQuest Pro software. Annexin V-positive/PI-negative cells were defined as early apoptotic cells, whereas Annexin V-positive/PI-positive cells were defined as late apoptotic or necrotic cells. The total apoptosis rate was calculated as the sum of these two populations.

Measurement of mitochondrial membrane potential

Mitochondrial membrane potential (delta psi m) was assessed using a JC-1 mitochondrial membrane-potential assay kit (Beyotime, Shanghai, China). HepG2 cells from different treatment groups were seeded in confocal culture dishes. After treatment, the culture medium was removed, and cells

were incubated with 10 microg/mL JC-1 working solution at 37°C for 20 min. Cells were then washed twice with PBS and observed using a Leica SP8 confocal microscope. In cells with high mitochondrial membrane potential, JC-1 forms J-aggregates that emit red fluorescence. In cells with reduced mitochondrial membrane potential, JC-1 mainly remains as monomers that emit green fluorescence. Changes in delta psi m were quantified by calculating the ratio of red to green fluorescence intensity.

Caspase-3/7 activity assay

Caspase-3/7 activity was measured using the Caspase-Glo 3/7 Assay Kit (Promega, Madison, WI, USA). HepG2 cells were seeded in 96-well plates at a density of 1 × 10^4 cells per well. After the corresponding treatments, 100 microL of Caspase-Glo 3/7 reagent was added to each well, gently mixed and incubated for 1 h at room temperature in the dark. Chemiluminescence intensity was then measured using a multimode microplate reader (Tecan, Männedorf, Switzerland).

Nude mouse xenograft model

All animal experiments were approved by the Animal Experimentation Ethics Committee of the Scientific Experiment Center of Guangxi University of Chinese Medicine and were conducted in accordance with laboratory animal welfare guidelines. Male BALB/c nude mice aged 4-5 weeks (Hunan SJA Laboratory Animal Co., Ltd.) were used to establish the xenograft model. HepG2 cells expressing shNC or shGRP75 (5 × 10^6 cells suspended in 100 microL PBS) were subcutaneously injected into the right axilla of each mouse. Tumour length (L) and width (W) were measured twice weekly using callipers, and tumour volume was calculated using the formula V = 0.5 × L × W^2.

When the mean tumour volume reached approximately 100 mm3, mice were assigned to groups according to tumour volume (n = 3 per group): shNC plus vehicle control, shGRP75 plus vehicle control, shNC plus sorafenib and shGRP75 plus sorafenib. Sorafenib (Selleck Chemicals) was administered by intraperitoneal injection once daily at 30 mg/kg, and control mice received an equal volume of vehicle. After 21 days of continuous treatment, mice were euthanized, and tumours were completely excised and weighed. Some tumour tissues were fixed in 4% paraformaldehyde for subsequent immunohistochemical analysis.

Immunohistochemical analysis

Paraffin-embedded tumour tissue sections were deparaffinized and rehydrated, followed by antigen retrieval using citrate buffer. Sections were incubated with 3% H2O2 for 10 min at room temperature to block endogenous peroxidase activity and then blocked with 5% BSA for 30 min. Sections were incubated overnight at 4°C with rabbit monoclonal antibodies against Ki-67 (CST, #9449, 1:400) or cleaved caspase-3 (CST, #9664, 1:400). The next day, sections were incubated with HRP-conjugated secondary antibody, developed using a DAB chromogenic kit and counterstained with haematoxylin.

TCGA-LIHC public database analysis

Standardized transcriptomic data and clinical information for the TCGA-LIHC cohort were downloaded from the UCSC Xena database. HSPA9 mRNA expression data were extracted from tumour tissues and adjacent normal tissues. R software was used to compare HSPA9 mRNA expression across tissue types, tumour stages and T stages. Patients were divided into high- and low-expression groups according to the median HSPA9 mRNA expression level. Kaplan-Meier analysis was used to generate overall-survival curves, and the log-rank test was used to compare survival between groups. Public database analyses were mainly performed using R software (version 4.3.1), and $P < 0.05$ was considered statistically significant.

Statistical analysis

Experimental data are presented as the mean +/- standard deviation (SD). Each in vitro experiment was independently repeated at least three times. The sample size for animal experiments is indicated in the corresponding figure legends. Statistical analyses were performed using GraphPad Prism 8.0. Comparisons between two groups were performed using two-tailed unpaired Student's t-tests. Comparisons among multiple groups were performed using one-way analysis of variance followed by Tukey's multiple-comparison test. $P < 0.05$ was considered statistically significant.

Results

HepG2 cells show tighter MERC morphology, and HSPA9 mRNA is upregulated in HCC datasets and associated with worse survival

To compare mitochondria-ER contacts between HCC cells and non-malignant liver epithelial cells, we examined MERC morphology in THLE-2 and HepG2 cells by TEM. HepG2 cells showed closer physical contacts between mitochondria and the ER than THLE-2 cells (Fig. 1A). Quantitative analysis confirmed a greater fraction of the mitochondrial perimeter occupied by MERCs and a shorter mean contact distance in HepG2 cells (Fig. 1B).

Analysis of the TCGA-LIHC cohort showed higher HSPA9 mRNA expression in HCC tumour tissues than in adjacent normal tissues. When patients were stratified by expression level, high HSPA9 expression was associated with worse overall survival (Fig. 1C). By contrast, HSPA9 mRNA expression did not show a consistent relationship with tumour stage or T stage. These findings indicate that HepG2 cells display tighter MERC morphology than THLE-2 cells and that HSPA9 is upregulated in public HCC transcriptomic data.

GRP75 manipulation shifts MERC morphology in HepG2 cells

To determine whether altered GRP75 expression was sufficient to remodel MERC structure, we next overexpressed or knocked down GRP75 in HepG2 cells. Transfection-marker fluorescence increased

gradually at 12, 24 and 48 h and reached a relatively high level at 48 h (Fig. 2A and Fig. 2C). We therefore selected 48 h as the main time point for subsequent structural and functional experiments.

TEM showed tighter mitochondria-ER contacts in the GRP75-overexpression group and looser MERC morphology in the GRP75-knockdown group (Fig. 2B). Compared with controls, GRP75 overexpression increased MERC contact length and shortened the mean contact distance. GRP75 knockdown reduced contact length and increased the mean contact distance (Fig. 2D). These reciprocal alterations indicate that GRP75 expression influences MERC structural coupling in HepG2 cells.

GRP75 manipulation alters mitochondrial Ca2 + transients

To test whether GRP75-associated MERC remodelling affected mitochondrial Ca2 + handling, we measured Rhod-2 AM fluorescence after ATP stimulation. Compared with controls, Rhod-2 AM transients were enhanced in the GRP75-overexpression group and attenuated in the GRP75-knockdown group (Fig. 3). Peak or intensity quantification matched the representative images, suggesting that GRP75 expression modulates mitochondrial Ca2 + uptake in HepG2 cells.

GRP75 manipulation alters apoptosis, mitochondrial membrane potential and mitochondrial apoptotic markers in sorafenib-treated HepG2 cells

To determine whether GRP75 status influences apoptotic susceptibility under sorafenib treatment, we assessed apoptosis in each group by Annexin V-FITC/PI flow cytometry. Total apoptosis differed among the treatment groups. Upon sorafenib challenge, apoptosis was lower in the GRP75-overexpression plus sorafenib group than in the sorafenib-alone group, whereas it increased further in the GRP75-knockdown group (Fig. 4A).

JC-1 staining showed increased green monomer fluorescence after sorafenib treatment, indicating reduced mitochondrial membrane potential. Upon sorafenib challenge, the GRP75-overexpression group retained stronger red aggregate fluorescence. By contrast, the GRP75-knockdown plus sorafenib group showed stronger green monomer fluorescence and greater loss of red aggregate fluorescence (Fig. 4B).

Western blotting and enzyme-activity assays supported these apoptotic readouts. During sorafenib treatment, Bax and cleaved caspase-3 expression were lower in the GRP75-overexpression group than in the sorafenib-alone group. GRP75 knockdown increased Bax and cleaved caspase-3 expression and reduced Bcl-2 expression (Fig. 4C and Fig. 4D). Caspase-3/7 activity was lower with GRP75 overexpression and higher with GRP75 knockdown (Fig. 4E). These results indicate that GRP75 expression modulates mitochondrial apoptotic sensitivity during sorafenib treatment.

GRP75 knockdown is associated with lower final xenograft burden and stronger sorafenib-associated pro-apoptotic marker expression

In the HepG2 xenograft model, endpoint tumour photographs and quantitative measurements showed lower tumour volume in the shGRP75 plus vehicle-control group than in the shNC plus vehicle-control group (Fig. 5A1 and Fig. 5A3). During sorafenib treatment, the shGRP75 plus sorafenib group had the lowest final tumour burden among the groups shown (Fig. 5A2 and Fig. 5A3).

qPCR analysis of tumour tissues confirmed lower HSPA9/GRP75 mRNA expression in the shGRP75 plus vehicle-control group than in the shNC plus vehicle-control group (Fig. 5B). Immunohistochemistry showed weaker Ki-67 immunoreactivity in the shGRP75 plus vehicle-control group (Fig. 5C1 and Fig. 5C3). During sorafenib treatment, cleaved caspase-3 immunoreactivity increased and was most pronounced in the shGRP75 plus sorafenib group (Fig. 5C2 and Fig. 5C3). These in vivo results were consistent with the in vitro apoptosis assays and support an association between GRP75 knockdown, reduced tumour burden and stronger sorafenib-associated pro-apoptotic marker expression.

Discussion

This study investigated whether GRP75-mediated MERC remodelling connects mitochondrial Ca2 + handling with apoptotic sensitivity to sorafenib in HepG2 cells. We found that HepG2 cells displayed tighter mitochondria-ER contacts than THLE-2 cells. HSPA9 mRNA was upregulated in HCC tissues in TCGA-LIHC data and was associated with worse overall survival, although it was not consistently related to tumour stage or T stage. In HepG2 cells, GRP75 manipulation produced coordinated alterations in MERC morphology, Rhod-2 AM transients, mitochondrial membrane potential and apoptotic sensitivity. Xenograft results further supported the functional relevance of this regulatory axis in tumour growth. Collectively, these observations position the GRP75-MERC axis as a functional rheostat that governs mitochondrial apoptotic commitment during sorafenib challenge, rather than a static structural correlate. However, the prognostic association of HSPA9 should not be interpreted as independent without multivariable Cox analysis and validation in independent cohorts.

MERCs/MAMs provide a structural basis for local communication between mitochondria and the ER [17–19]. Through these contact sites, cells coordinate Ca2 + signalling, cell-death regulation, lipid exchange, mitochondrial dynamics and ER stress [16–20]. Here, HepG2 cells showed a greater fraction of the mitochondrial perimeter occupied by MERCs and a shorter mean contact distance, indicating tighter organelle contacts in this model. Previous studies have shown that MAM/MERC remodelling can affect cancer-cell homeostasis, lipid peroxidation, cell-death sensitivity and treatment response [21, 22, 26]. Because this study compared only HepG2 and THLE-2 cells, these morphological differences should be interpreted as findings within the HepG2 model rather than a general feature of HCC cells.

The known function of GRP75 provides a plausible explanation for these structural alterations. As a chaperone in the IP3R-GRP75-VDAC1 complex, GRP75 promotes functional coupling between ER IP3R and mitochondrial outer-membrane VDAC1 [23]. Recent studies emphasize that MERCs are not determined by a single complex. Instead, they form a dynamic network regulated by multiple tethering proteins, membrane proteins and stress signals [24]. In our experiments, GRP75 overexpression

increased MERC contact and shortened the mean distance, whereas GRP75 knockdown produced the opposite pattern. This finding is consistent with the bridging role of GRP75 in maintaining ER-mitochondria contacts. Other tethering molecules and pathways, including MFN2, the VAPB-PTPIP51 complex, and RMDN3/PTPIP51-mediated signalling, also regulate ER-mitochondria tethering [36–39]. These molecules may compensate for changes in GRP75 expression, indicating that MERC remodelling is unlikely to be driven by one protein alone. Even so, the reciprocal alterations observed after GRP75 overexpression and knockdown place GRP75 at an important position in maintaining ER-mitochondria contact stability.

The Ca2 + data connect GRP75-associated MERC remodelling with mitochondrial functional state. Rhod-2 AM assays showed enhanced mitochondrial Ca2 + transients in the GRP75-overexpression group and attenuated transients in the GRP75-knockdown group. Earlier work connected close ER-mitochondria contacts with mitochondrial Ca2 + responses [16], and recent reviews have emphasized the role of MAMs/MERCs in Ca2 + transport and disease-associated signalling [20]. GRP75-mediated IP3R-VDAC1 coupling provides a molecular basis for local Ca2 + transfer [23, 24]. However, Rhod-2 AM fluorescence intensity can be affected by probe loading, mitochondrial uptake/retention, and mitochondrial membrane potential. Therefore, the fluorescence alterations observed here cannot be equated directly with complete ER-mitochondria Ca2 + flux. Considering MERC structure, Rhod-2 AM fluorescence, JC-1 membrane potential and apoptotic readouts together, GRP75 may raise the apoptotic threshold of HepG2 cells following sorafenib exposure by maintaining MERC-associated mitochondrial Ca2 + handling and mitochondrial function. Direct measurement of ER-mitochondria Ca2 + flux will be needed to validate this mechanism.

The apoptosis results indicate that GRP75 status affects the susceptibility of HepG2 cells to mitochondrial apoptosis during sorafenib treatment. Drug resistance in HCC entails multiple cell-death pathways and adaptive remodelling [15]. In sorafenib-related models, ER stress, RAF1/MEK/ERK signalling and BCL-2 family proteins can influence apoptotic responses or resistant states [32–34]. ER-mitochondria crosstalk, SMG5 inhibition, caspase-3/SREBP2-mediated cholesterol biosynthesis and AKR1C3-dependent lipid-droplet formation have also been implicated in sorafenib resistance or adaptation to targeted therapy [35, 40–42]. In our study, GRP75 knockdown during sorafenib treatment increased the proportion of Annexin V/PI-positive cells, reduced mitochondrial membrane potential, enhanced Bax and cleaved caspase-3 expression and decreased Bcl-2 expression. Conversely, GRP75 overexpression conferred a relative protective effect against sorafenib-induced mitochondrial injury. Together with the MERC and Rhod-2 AM findings, these data support a model in which GRP75-maintained ER-mitochondria coupling stabilizes mitochondrial function and makes cells less likely to cross the mitochondrial apoptotic threshold during sorafenib exposure. When GRP75 is reduced, looser MERC morphology, weaker mitochondrial Ca2 + transients and loss of membrane potential may jointly lower this threshold and amplify sorafenib-induced apoptotic signalling. This remains a mechanistic model, because mitochondrial metabolism, ER stress and drug responses after GRP75 rescue have not yet been directly tested.

The in vivo experiments provide tissue-level evidence that complements the cell-based findings. In the HepG2 xenograft model, GRP75 knockdown reduced final tumour burden and lowered Ki-67 immunoreactivity in tumour tissues. This suggests that reduced GRP75 may weaken tumour-cell proliferative capacity in vivo, in addition to affecting apoptotic readouts in vitro. During sorafenib treatment, cleaved caspase-3 immunoreactivity increased further, indicating that GRP75 knockdown may sensitize tumour tissues to drug-induced apoptosis. These findings were consistent with the in vitro observations of looser MERC morphology, weaker mitochondrial Ca2 + transients, reduced membrane potential and enhanced pro-apoptotic markers. The current in vivo experiments were mainly based on endpoint tumour burden, HSPA9/GRP75 mRNA and IHC markers. They should therefore be viewed as supportive evidence for in vitro-in vivo consistency and as mechanistic clues, rather than as a complete in vivo efficacy assessment. Future studies should use more systematic pharmacodynamic and mechanistic validation to test the stability of this axis across HCC models and treatment conditions.

Several limitations should be emphasized. First, the in vitro experiments were mainly based on a two-dimensional HepG2 culture model. HepG2 cells do not fully represent clinical HCC in drug-metabolizing enzyme expression, tumour heterogeneity or microenvironmental complexity [43, 44]. Second, beyond its role in IP3R-VDAC1-mediated ER-mitochondria tethering, GRP75 also functions as a molecular chaperone involved in proteostasis and stress adaptation. Enhanced apoptosis after GRP75 knockdown may therefore result from MERC structural alterations together with other GRP75-dependent effects. This issue should be clarified using approaches such as GRP75 rescue. Third, Rhod-2 AM imaging provided mitochondrial Ca2 + transients, but complete ER-mitochondria Ca2 + transfer flux requires more precise measurement. Finally, sorafenib is a multitarget drug, and the GRP75-MERC axis may explain only part of the mitochondrial apoptosis-related response. Future studies should examine this axis in more complex HCC models [45] and test its causal relationship with mitochondrial metabolism, oxidative stress and drug-induced apoptosis.

Conclusions

In summary, this study shows that the GRP75-MERC axis contributes to apoptosis regulation in HCC cells. GRP75 knockdown in HepG2 cells was associated with looser MERC morphology, weaker mitochondrial Ca2 + transients, reduced membrane potential and enhanced pro-apoptotic markers. Endpoint observations in vivo showed the same overall trend. These findings offer an organelle-contact perspective on apoptosis regulation in HCC cells and provide an experimental basis for further analysis of the GRP75-MERC axis in HCC treatment response.

Abbreviations

Bcl-2: B-cell lymphoma 2; GRP75: glucose-regulated protein 75; HCC: hepatocellular carcinoma; HSPA9: heat shock protein family A member 9; IP3R: inositol 1,4,5-trisphosphate receptor; JC-1: 5,5',6,6'-tetrachloro-1,1',3,3'-tetraethylbenzimidazolylcarbocyanine iodide; MAM: mitochondria-associated membrane; MERC: mitochondria-endoplasmic reticulum contact; qRT-PCR: quantitative real-time PCR;

TCGA-LIHC: The Cancer Genome Atlas Liver Hepatocellular Carcinoma; TEM: transmission electron microscopy; VDAC1: voltage-dependent anion channel 1.

Declarations

Ethics approval and consent to participate

This study was reviewed and approved by the Animal Experimentation Ethics Committee of Guangxi University of Chinese Medicine (approval No. GXTCMU-EC KS20260416-06). Consent to participate was not applicable.

Consent for publication

Not applicable.

Availability of data and materials

The dataset(s) supporting the conclusions of this article is(are) included within the article and its additional file(s). Public TCGA-LIHC data analyzed in this study are available from the UCSC Xena database.

Competing interests

The authors declare that they have no competing interests.

Funding

This work was supported by grants from the National Natural Science Foundation of China (No. 82560931), the Guangxi Natural Science Foundation Project (General Project, Special Programme on Traditional Chinese Medicine and Zhuang-Yao Medicine; No. 2025GXNSFAA069382) and the Engineering Research Center of Innovative Drug of Traditional Chinese and Zhuang Yao Medicine, Ministry of Education, Guangxi University of Chinese Medicine (No. ZYZYY25019).

Authors' contributions

XZ contributed to conceptualization, methodology, study design, experimental validation, formal analysis, funding acquisition, original drafting, and manuscript review and editing. ZJ contributed to experimental validation, data curation, formal analysis, literature retrieval, visualization, and manuscript review and editing. LC contributed to experimental validation, data curation, formal analysis, literature retrieval, visualization, and manuscript review and editing. JL, QH, LL, BL and YY contributed to data curation, formal analysis, literature retrieval, visualization, and manuscript review and editing. DZ contributed to conceptualization, supervision, project administration, and manuscript review and editing. XZ and DZ confirm the authenticity of the raw data. All authors read and approved the final manuscript.

Acknowledgements

The authors thank the public platform of the Scientific Experiment Center of Guangxi University of Chinese Medicine for providing instruments and technical support. The authors also thank Ms Ling Zhang for technical guidance.

References

1. Sung H, Ferlay J, Siegel RL, et al. Global Cancer Statistics 2020: GLOBOCAN Estimates of Incidence and Mortality Worldwide for 36 Cancers in 185 Countries. CA Cancer J Clin. 2021;71(3):209–49.
2. Rumgay H, Arnold M, Ferlay J, et al. Global burden of primary liver cancer in 2020 and predictions to 2040. J Hepatol. 2022;77(6):1598–606.
3. Singal AG, Kanwal F, Llovet JM. Global trends in hepatocellular carcinoma epidemiology: implications for screening, prevention and therapy. Nat reviews Clin Oncol. 2023;20(12):864–84.
4. Llovet JM, Kelley RK, Villanueva A, et al. Hepatocellular carcinoma. Nat Rev Dis Primers. 2021;7(1):6.
5. Vogel A, Meyer T, Sapisochin G, et al. Hepatocellular carcinoma Lancet. 2022;400(10360):1345–62.
6. Yang X, Yang C, Zhang S, et al. Precision treatment in advanced hepatocellular carcinoma. Cancer Cell. 2024;42(2):180–97.
7. Llovet JM, Ricci S, Mazzaferro V, et al. Sorafenib in advanced hepatocellular carcinoma. N Engl J Med. 2008;359(4):378–90.
8. Cheng AL, Kang YK, Chen Z, et al. Efficacy and safety of sorafenib in patients in the Asia-Pacific region with advanced hepatocellular carcinoma: a phase III randomised, double-blind, placebo-controlled trial. Lancet Oncol. 2009;10(1):25–34.
9. Cheng AL, Qin S, Ikeda M, et al. Updated efficacy and safety data from IMbrave150: Atezolizumab plus bevacizumab vs. sorafenib for unresectable hepatocellular carcinoma. J Hepatol. 2022;76(4):862–73.
10. Rimassa L, Finn RS, Sangro B. Combination immunotherapy for hepatocellular carcinoma. J Hepatol. 2023;79(2):506–15.
11. Zhu AX, Abbas AR, De Galarreta MR, et al. Molecular correlates of clinical response and resistance to atezolizumab in combination with bevacizumab in advanced hepatocellular carcinoma. Nat Med. 2022;28(8):1599–611.
12. Singal AG, Llovet JM, Yarchoan M, et al. AASLD Practice Guidance on prevention, diagnosis, and treatment of hepatocellular carcinoma. Hepatology. 2023;78(6):1922–65.
13. Taddei TH, Brown DB, Yarchoan M, Mendiratta-Lala M, Llovet JM. Critical Update: AASLD Practice Guidance on prevention, diagnosis, and treatment of hepatocellular carcinoma. Hepatology. 2025;82(1):272–4. 10.1097/HEP.0000000000001269.
14. Cappuyns S, Corbett V, Yarchoan M, et al. Critical appraisal of guideline recommendations on systemic therapies for advanced hepatocellular carcinoma: a review. JAMA Oncol. 2024;10(3):395–

404.
15. Ladd AD, Duarte S, Sahin I, et al. Mechanisms of drug resistance in HCC. Hepatology. 2024;79(4):926–40.
16. Rizzuto R, Pinton P, Carrington W, et al. Close contacts with the endoplasmic reticulum as determinants of mitochondrial Ca2 + responses. Science. 1998;280(5370):1763–6.
17. Barazzuol L, Giamogante F, Calì T. Mitochondria Associated Membranes (MAMs): Architecture and physiopathological role. Cell Calcium. 2021;94:102343.
18. Mao H, Chen W, Chen L, et al. Potential role of mitochondria-associated endoplasmic reticulum membrane proteins in diseases. Biochem Pharmacol. 2022;199:115011.
19. Roy R, Adhikary A, De R, et al. Mitochondria-ER crosstalk via MAMS: Bridging cellular homeostasis and cancer progression. Apoptosis. 2026;31(1):43.
20. Zhao W, Sheng R. The correlation between mitochondria-associated endoplasmic reticulum membranes (MAMs) and Ca2 + transport in the pathogenesis of diseases. Acta Pharmacol Sin. 2025;46(2):271–91.
21. Sassano ML, Tyurina YY, Diokmetzidou A, et al. Endoplasmic reticulum-mitochondria contacts are prime hotspots of phospholipid peroxidation driving ferroptosis. Nat Cell Biol. 2025;27(6):902–17.
22. Zhang Z, Zhou H, Gu W, et al. CGI1746 targets σ1R to modulate ferroptosis through mitochondria-associated membranes. Nat Chem Biol. 2024;20(6):699–709.
23. Szabadkai G, Bianchi K, Várnai P, et al. Chaperone-mediated coupling of endoplasmic reticulum and mitochondrial Ca2 + channels. J Cell Biol. 2006;175(6):901–11.
24. Atakpa-Adaji P, Ivanova A. IP3R at ER-Mitochondrial Contact Sites: Beyond the IP3R-GRP75-VDAC1 Ca2 + Funnel. Contact. 2023;6:25152564231181020.
25. Tiwary S, Nandwani A, Khan R, et al. GRP75 mediates endoplasmic reticulum-mitochondria coupling during palmitate-induced pancreatic beta-cell apoptosis. J Biol Chem. 2021;297(6):101368.
26. Li J, Qi F, Su H, et al. GRP75-faciliated mitochondria-associated ER membrane (MAM) integrity controls cisplatin-resistance in ovarian cancer patients. Int J Biol Sci. 2022;18(7):2914.
27. Jin M, Yang Y, Dai Y, et al. 27-Hydroxycholesterol is a specific factor in the neoplastic microenvironment of HCC that causes MDR via GRP75 regulation of the redox balance and metabolic reprogramming. Cell Biol Toxicol. 2022;38(2):311–24.
28. Yang Y, Jin M, Dai Y, et al. Involvement and targeted intervention of mortalin-regulated proteome phosphorylated-modification in hepatocellular carcinoma. Front Oncol. 2021;11:687871.
29. Esfahanian N, Knoblich CD, Bowman GA, et al. Mortalin: Protein partners, biological impacts, pathological roles, and therapeutic opportunities. Front Cell Dev Biology. 2023;11:1028519.
30. Wang Z, Zhu J, Wang Z, et al. Intelligent identification and targeted intervention of GRP75-caused drug resistant hepatocellular carcinoma, a study based on radiomics, machine learning, and molecular pharmacology. Int J Surg. 2026;112(5):11376–92.

31. Ko M, Kim J, Lazim R, et al. The anticancer effect of metformin targets VDAC1 via ER-mitochondria interactions-mediated autophagy in HCC. Exp Mol Med. 2024;56(12):2714–25.
32. Wang X, Hu R, Song Z, et al. Sorafenib combined with STAT3 knockdown triggers ER stress-induced HCC apoptosis and cGAS-STING-mediated anti-tumor immunity. Cancer Lett. 2022;547:215880.
33. Wu S, Hong Y, Li H, et al. SHBs Mitigates Sorafenib-Induced Apoptosis in Hepatocellular Carcinoma via Activation of RAF1/MEK/ERK Signaling Pathway. Cancer Sci. 2025;116(9):2471–85.
34. de Melo Silva AJ, de Melo Gama JE, de Oliveira SA. The role of Bcl-2 family proteins and sorafenib resistance in hepatocellular carcinoma. Int J Cell Biology. 2024;2024(1):4972523.
35. Lin Y, Zhang F, Guo W et al. Hyperbaric oxygen targets RCN1 to modulate ER-mitochondria crosstalk and ameliorate sorafenib resistance in hepatocellular carcinoma. Drug Resist Updates, 2025: 101342.
36. Hu Y, Chen H, Zhang L, et al. The AMPK-MFN2 axis regulates MAM dynamics and autophagy induced by energy stresses. Autophagy. 2021;17(5):1142–56.
37. Stoica R, De Vos KJ, Paillusson S, et al. ER-mitochondria associations are regulated by the VAPB-PTPIP51 interaction and are disrupted by ALS/FTD-associated TDP-43. Nat Commun. 2014;5(1):3996.
38. Jiang T, Ruan N, Luo P, et al. Modulation of ER-mitochondria tethering complex VAPB-PTPIP51: novel therapeutic targets for aging-associated diseases. Ageing Res Rev. 2024;98:102320.
39. Shiiba I, Ito N, Oshio H, et al. ER-mitochondria contacts mediate lipid radical transfer via RMDN3/PTPIP51 phosphorylation to reduce mitochondrial oxidative stress. Nat Commun. 2025;16(1):1508.
40. Fang N, Liu B, Pan Q, et al. SMG5 inhibition restrains hepatocellular carcinoma growth and enhances sorafenib sensitivity. Mol Cancer Ther. 2024;23(8):1188–200.
41. Mok EHK, Leung CON, Zhou L, et al. Caspase-3-induced activation of SREBP2 drives drug resistance via promotion of cholesterol biosynthesis in hepatocellular carcinoma. Cancer Res. 2022;82(17):3102–15.
42. Wu C, Dai C, Li X, et al. AKR1C3-dependent lipid droplet formation confers hepatocellular carcinoma cell adaptability to targeted therapy. Theranostics. 2022;12(18):7681.
43. Stanley LA, Wolf CR. Through a glass, darkly? HepaRG and HepG2 cells as models of human phase I drug metabolism. Drug Metab Rev. 2022;54(1):46–62.
44. Arzumanian VA, Kiseleva OI, Poverennaya EV. The curious case of the HepG2 cell line: 40 years of expertise. Int J Mol Sci. 2021;22(23):13135.
45. Ali ASM, Wu D, Bannach-Brown A, et al. 3D bioprinting of liver models: A systematic scoping review of methods, bioinks, and reporting quality. Mater Today Bio. 2024;26:100991.

Figures

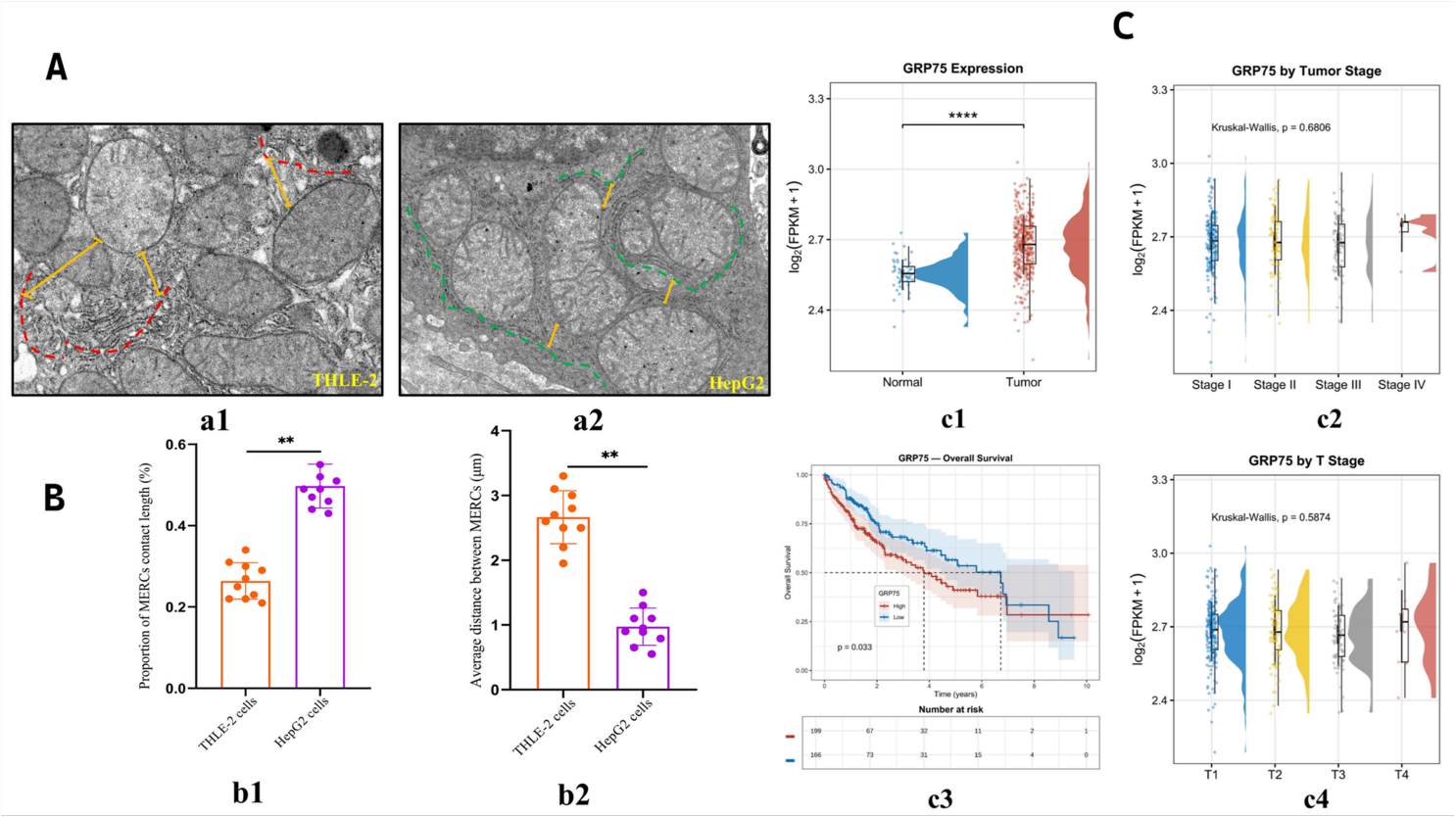


Figure 1

HepG2 cells show tighter MERC morphology, and HSPA9 mRNA is upregulated in HCC datasets and associated with worse survival.

(A) Representative TEM images of mitochondria-ER contacts in THLE-2 and HepG2 cells. Dashed lines indicate mitochondrial regions, and arrows indicate adjacent mitochondria-ER contact sites.

(B) Quantitative analysis of the fraction of the mitochondrial perimeter occupied by MERCs and mean contact distance in THLE-2 and HepG2 cells. Data are presented as the mean +/- SD, n = 8.

(C) HSPA9 mRNA expression and clinical correlation analysis in the TCGA-LIHC cohort. c1, HSPA9 mRNA expression in normal and tumour tissues; c2, HSPA9 mRNA expression across tumour stages; c3, overall-survival analysis stratified by HSPA9 mRNA expression; c4, HSPA9 mRNA expression across T stages. "GRP75" in this panel refers to HSPA9 transcript levels, not GRP75 protein expression. *P < 0.05, **P < 0.01, ***P < 0.001; ns, not significant.

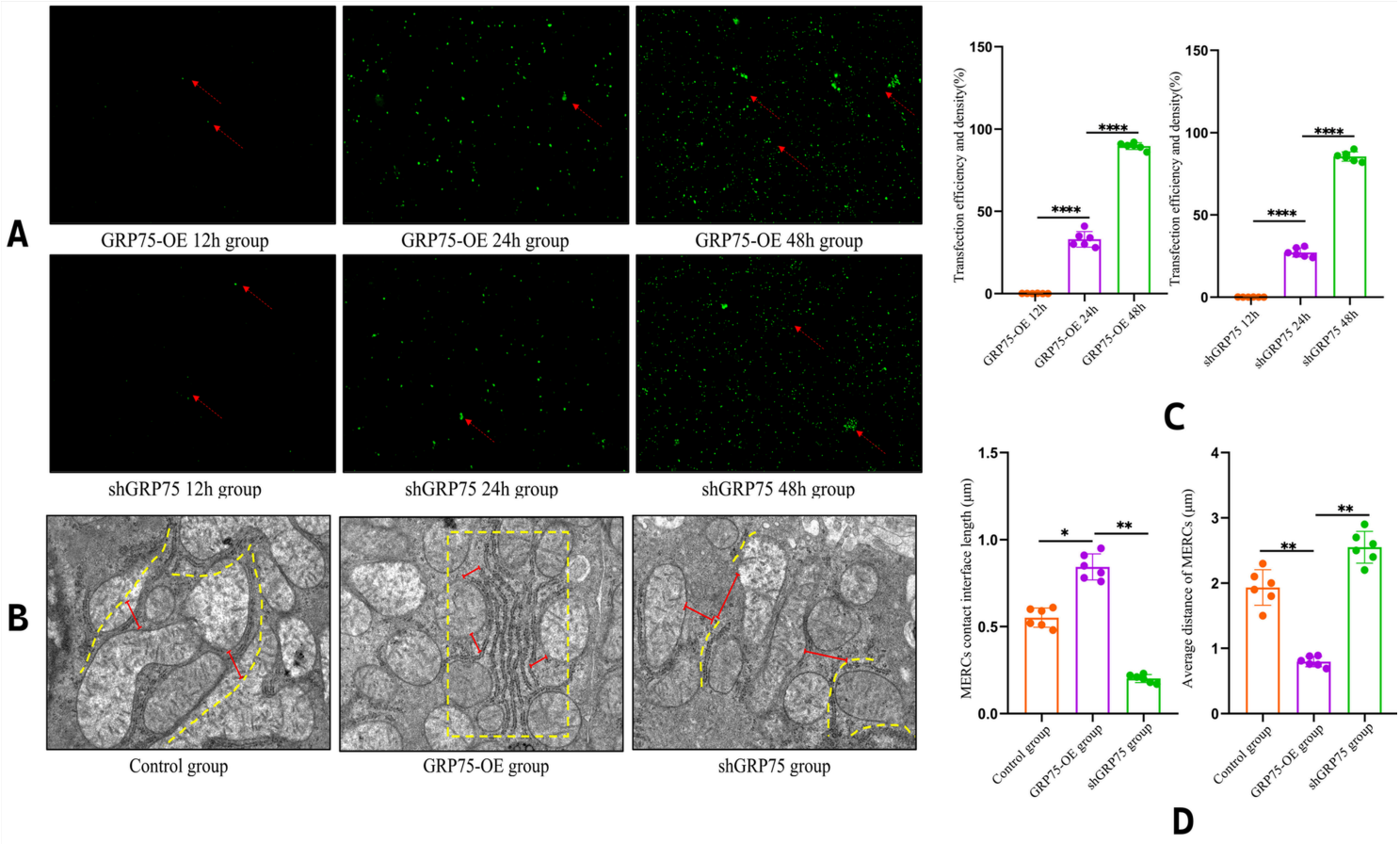


Figure 2

GRP75 manipulation shifts MERC morphology in HepG2 cells.

(A) Representative fluorescence images of transfection marker signals at 12, 24 and 48 h after GRP75 overexpression or shGRP75 transfection. Arrows indicate representative positive fluorescence signals.

(B) Representative TEM images of MERC morphology in control, GRP75-overexpression and GRP75-knockdown HepG2 cells. Dashed lines indicate mitochondria and mitochondria-ER contact regions, and arrows indicate local contact distance or adjacent contact sites.

(C) Quantitative analysis of transfection marker signal intensity/density at different time points after GRP75 overexpression or shGRP75 transfection. Data are presented as the mean +/- SD, n = 6.

(D) Quantitative analysis of MERC contact length and mean contact distance in the control, GRP75-overexpression and GRP75-knockdown groups. Data are presented as the mean +/- SD, n = 6. *P < 0.05, **P < 0.01, ***P < 0.001; ns, not significant.

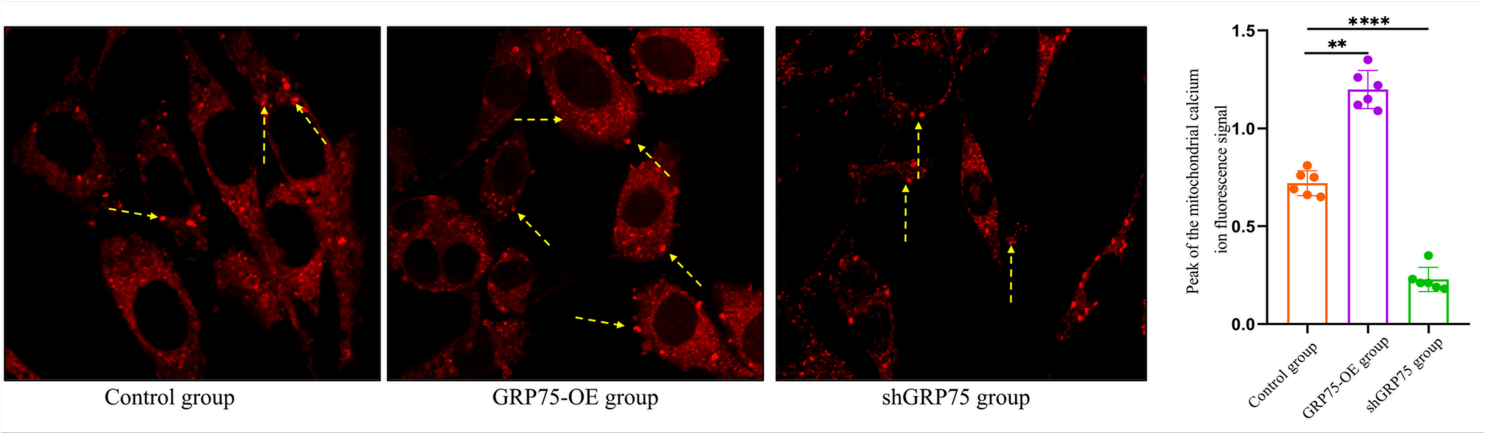


Figure 3

GRP75 manipulation alters mitochondrial Ca2+ transients.

Representative confocal images and peak/intensity quantification of Rhod-2 AM fluorescence transients in control, GRP75-overexpression and GRP75-knockdown HepG2 cells after ATP stimulation. Arrows indicate representative Rhod-2 AM fluorescence. Data are presented as the mean +/- SD, n = 6. Significance markers are shown in the corresponding panel. *P < 0.05, **P < 0.01, ***P < 0.001; ns, not significant.

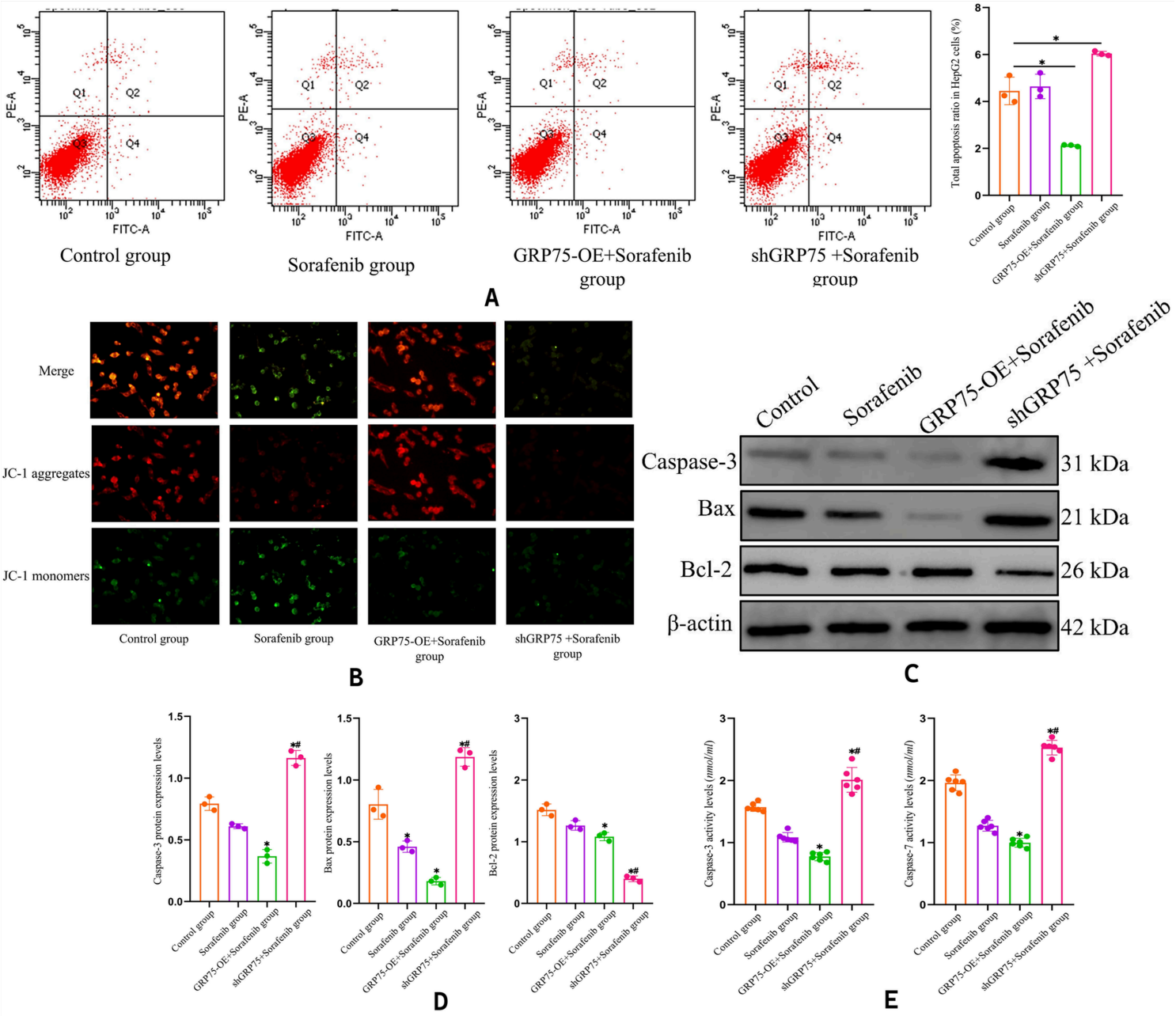


Figure 4

GRP75 manipulation alters apoptosis, mitochondrial membrane potential and mitochondrial apoptotic markers in sorafenib-treated HepG2 cells.

(A) Annexin V-FITC/PI flow cytometry was used to assess apoptosis in the control, sorafenib-treated, GRP75-overexpression plus sorafenib and GRP75-knockdown plus sorafenib groups. Total apoptosis was calculated as the sum of early and late apoptotic cells. Data are presented as the mean +/- SD, n = 6.

(B) JC-1 staining was used to assess mitochondrial membrane-potential changes in each group. Red fluorescence represents JC-1 aggregates, and green fluorescence represents JC-1 monomers.

(C) Western blot analysis of cleaved caspase-3, Bax, Bcl-2 and beta-actin protein expression in each group.

(D) Quantitative analysis of cleaved caspase-3, Bax and Bcl-2 protein expression from western blots. Data are presented as the mean +/- SD, n = 3.

(E) Caspase-3 and Caspase-7 activity assays in each group. Data are presented as the mean +/- SD, n = 6. *P < 0.05, **P < 0.01, ***P < 0.001; ns, not significant.

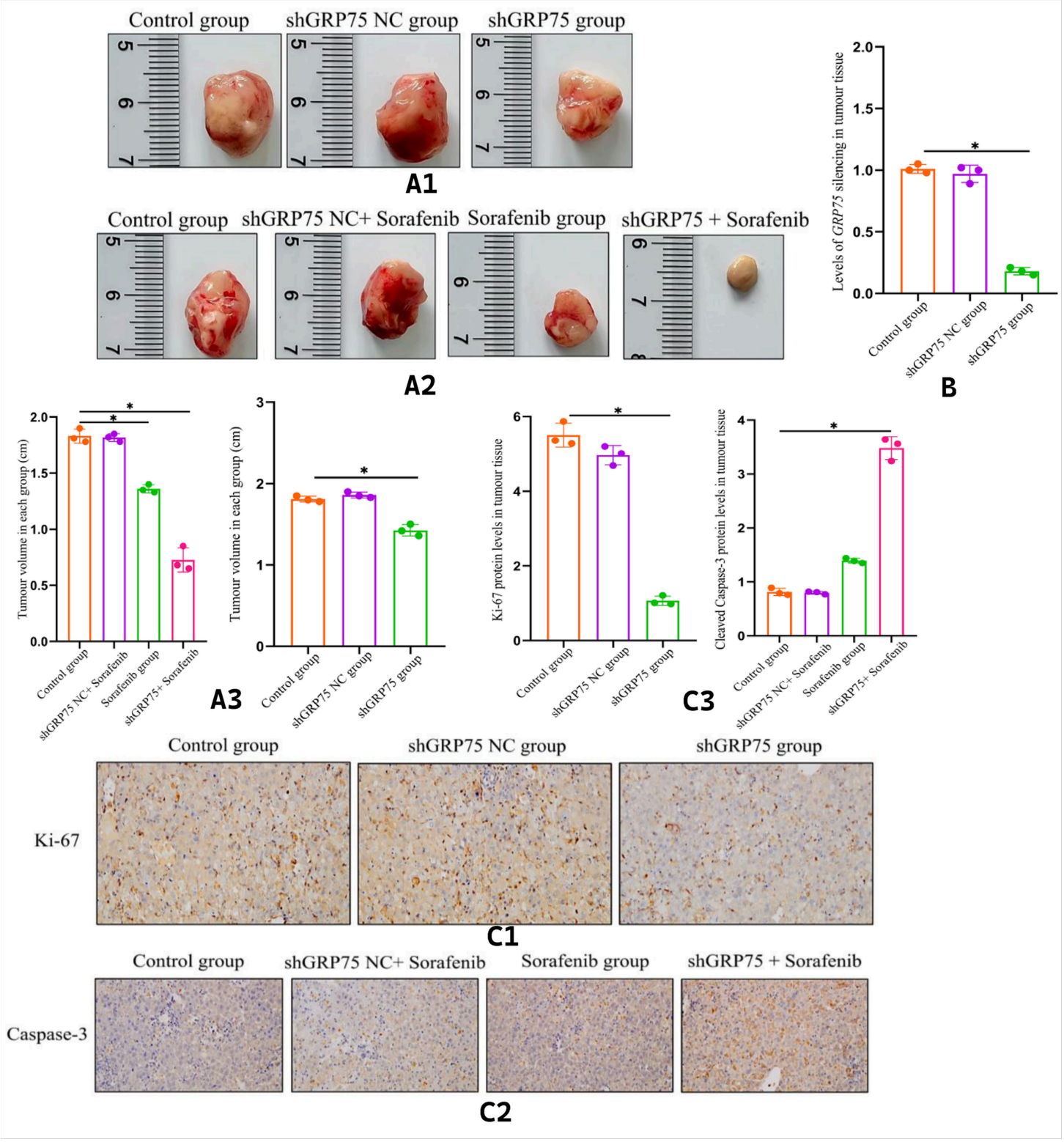


Figure 5

GRP75 knockdown is associated with lower final xenograft burden and stronger sorafenib-associated pro-apoptotic marker expression.

(A1) Representative endpoint excised tumours from the shNC plus vehicle-control and shGRP75 plus vehicle-control groups. The shGRP75 NC group shown in the figure corresponds to the shNC control

described in the text.

(A2) Representative endpoint excised tumours from the control, shGRP75 negative-control plus sorafenib, sorafenib-alone and shGRP75 plus sorafenib groups. In the figure, shGRP75 NC+Sorafenib refers to the sorafenib-treated group with negative-control transfection.

(A3) Quantitative analysis of endpoint tumour volume in the groups shown in A1 and A2. Data are presented as the mean +/- SD, n = 3.

(B) qPCR analysis of HSPA9/GRP75 mRNA expression in tumour tissues from the shNC plus vehicle-control and shGRP75 plus vehicle-control groups, used to assess the in vivo level of GRP75 knockdown. Data are presented as the mean +/- SD, n = 3.

(C1) Representative Ki-67 immunohistochemical staining of xenograft tumour tissues from the shNC plus vehicle-control and shGRP75 plus vehicle-control groups.

(C2) Representative cleaved caspase-3 immunohistochemical staining in the control, shGRP75 negative-control plus sorafenib, sorafenib-alone and shGRP75 plus sorafenib groups.

(C3) Quantitative analysis of Ki-67 and cleaved caspase-3 immunoreactivity. Data are presented as the mean +/- SD, n = 3. *P < 0.05, **P < 0.01, ***P < 0.001; ns, not significant.